(39) Mills, P. J.; Mayer, J. W.; Kramer, E. J.; Hadziioannou, G.; Lutz, P.; Strazielle, C.; Rempp, P.; Kovacs, A.—Abstract submitted for APS meeting, Baltimore, March 1985. Also Poster—Gordon Polymer Physics Conference, July 1984.
(40) For example, $\tau_c = (1/6)\tau_{rep}(p)$ in the calculation of ref 17.
(41) I am indebted to Prof. de Gennes for discussions concerning this approach.
(42) A is of order $\alpha(f-2)$ for large N.
(43) Following submission of this paper we became aware of recent work by N. Hadjichristidis and J. Roovers (*Polymer*, in press) indicating that the viscosity of four-arm polybutadiene (PBD) stars is indeed some 25% higher than for three-arm PBD stars with identical arms, a trend that appears to support our prediction.
(44) J. Roovers has just published (*Macromolecules* **1985**, *18*, 1359) viscosity–molecular weight data for ring–polystyrene melts.

Brownian Dynamics Simulation of Wormlike Chains. Fluorescence Depolarization and Depolarized Light Scattering

Stuart A. Allison

Department of Chemistry, Georgia State University, Atlanta, Georgia 30303.
Received May 3, 1985

ABSTRACT: Brownian dynamics is used to simulate fluorescence depolarization and depolarized light scattering from a discrete wormlike chain model. Flexible constraints are used to hold adjacent subunits at a nearly constant separation. "Experiments" with rigid and flexible constraints were essentially identical. Preaveraging hydrodynamic interaction was found to have a negligible effect on 10-subunit chains for the experiments carried out in this work. Simulations on 30-subunit chains were carried out with preaveraging. Fluorescence depolarization was observed to be more sensitive to internal motion than depolarized light scattering. The fluorescence depolarization was also found to be very sensitive to the persistence length. Excellent agreement between the Barkley–Zimm theory of bending (Barkley, M. D.; Zimm, B. H. *J. Chem. Phys.* **1979**, *70*, 2991) and the fluorescence depolarization simulations was also obtained.

I. Introduction

Computer simulations of long-range motion in macromolecules have increased greatly in recent years. Because these motions are generally slow, techniques other than conventional molecular dynamics must be used to study them. Brownian dynamics simulation methods have proven to be particularly useful in this regard.[1-4] To cite a few applications, they have been used to study backbone motion and isomerization in simple chain molecules,[5-9] hinge bending[10] and helix–coil transitions[11] in proteins, ring-closure dynamics in alkane chains,[12] biomolecular diffusion-controlled reactions,[13,14] transport properties of rigid and flexible macromolecules,[15] and fluorescence depolarization from hinged macromolecules[16] as well as DNA restriction fragments.[17] Brownian dynamics is an appropriate method for highly damped systems and is the diffusional analogue of molecular dynamics. The simulation is carried out by numerical integration of the Langevin equation.[2-4] The solvent is represented by suitable frictional and random forces and possibly by modified potentials of mean force. A recent review by McCammon gives a clear physical picture of Brownian motion in the context of protein dynamics.[18]

The focus of this article is the bending and overall motions of wormlike chains. Wormlike chains are realistic models for stiff linear polymers like DNA. Analytic theories of Gaussian or Rouse–Zimm model chains, as pioneered by Kirkwood[19] and Zimm,[20] have been successful in interpreting long-time (low-frequency) experiments on high molecular weight polymers. These models are, however, inadequate when the short-time or high-frequency behavior is of interest. Dielectric dispersion, fluorescence depolarization, NMR, depolarized light scattering, and perhaps polarized dynamic light scattering at a large scattering vector are several experimental methods that probe rapid internal motions of polymers.

The fluorescence anisotropy decay of ethidium bromide bound to DNA is an illustrative example of rapid internal motion in stiff polymers.[21-24] Because the emission dipole of the dye is tilted by about 70° from the local helix axis, torsional rather than bending motions are primarily responsible for this depolarization. Nonetheless, the latter motions do contribute. Analytic theories by Barkley and Zimm,[25] and by Allison and Schurr,[26] as well as a recent analysis by Yoshizaki et al.,[27,28] accurately reproduce the nonexponential decay. Hence, the experiments appear to confirm the theories with regard to torsional motion. In addition to torsion, the theories of Barkley and Zimm[25] and Yoshizaki, Yamakawa, and co-workers[27,28] account for bending as well. Unfortunately, it has not been possible to study bending motions directly (in the absence of torsion) by fluorescence depolarization, since this would require the bound chromophore to have its emission dipole parallel to the local helix axis. An alternative is to carry out computer "experiments" on well-defined model systems.

In this work, the technique of Brownian dynamics is used to simulate fluorescence depolarization from a discrete wormlike chain model of DNA in which the emission dipole is in a parallel configuration. Depolarized light scattering is also illustrated. Chains made up of 10 or 30 subunits are used where the longer chains have a contour length of about 920 Å. For 10-subunit chains, simulations with preaveraged and without preaveraged hydrodynamic interaction are compared and shown to be in good agreement with each other. This is consistent with the results of Garcia de la Torre and co-workers.[29] All simulations on 30-subunit chains have preaveraged hydrodynamic interaction.

In the next section, we first present the discrete wormlike chain model. The Brownian dynamics algorithm is briefly described along with the treatments of hydrodynamic interaction that are used. A description of how one simulates a particular experiment concludes this section. In section III, we first examine the effects of varying the stretching force constant and preaveraged hydrodynamic

0024-9297/86/2219-0118$01.50/0

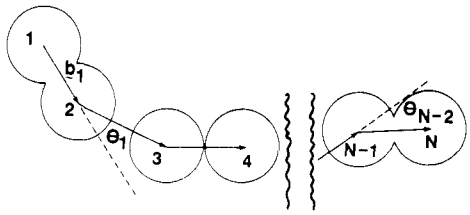

Figure 1. Discrete wormlike chain model. The chain consists of N beads that are not necessarily touching because of harmonic stretching forces.

interaction on fluorescence depolarization from 10-subunit chains. This is followed by simulated experiments on 30-subunit chains. The dependence of fluorescence depolarization (fd) on the location of the chromophore and the persistence length is examined. Also, a comparison between the simulations and the Barkley–Zimm theory is made. A simulation of depolarized light scattering is described at the end of this section. In section IV, the main conclusions of this work are summarized.

II. Methodology

The discrete wormlike chain (wlc) model used in this work is shown schematically in Figure 1. N beads of radius a are linked end-to-end by $N-1$ virtual bonds. A bead radius of 15.9 Å was used, since this choice accurately mimics the overall rotational diffusion of DNA modeled as a continuous wlc cylinder (radius = 13 Å).[30] Initial configurations were randomly generated with a slightly modified version of the Hagerman–Zimm algorithm[30] in which the interbead spacing is allowed to vary. The average interbead spacing was chosen to be $2a$ (corresponding to touching beads), while the variance is given by

$$\langle (b_j - 2a)^2 \rangle = k_B T/h \tag{1}$$

where $b_j = |\mathbf{b}_j|$ is the interbead spacing between subunits j and $j+1$, k_B is Boltzmann's constant, T is the absolute temperature, and h is a stretching force constant described in more detail below. Initially b_j is assigned a value of $2a + (k_B T/h)^{1/2} X$, where X is a Gaussian random number of 0 mean and variance 1. In most simulations h was chosen sufficiently large so that $(b_j - 2a)/2a \ll 1$. In order to check the chain generation procedure, computed values of the mean-squared end-to-end distance averaged over an ensemble (typically several hundred) of computer-generated chains were compared with known analytic solutions.[17,30] Agreement was always within a few percent.

In Brownian dynamics, one needs to know the direct forces acting on all subunits. For the discrete wlc model, direct forces due to stretching and bending must be considered. They were derived from stretching (U^s) and bending (U^b)[31] potentials

$$U^s = (h/2) \sum_{j=1}^{N-1} (b_j - 2a)^2 \tag{2}$$

$$U^b = (g/2) \sum_{j=1}^{N-2} \theta_j^2 \tag{3}$$

where g is the bending force constant and θ_j is the angle between virtual bond vectors j and $j+1$. The persistence length, P, is related to g by the expression[31]

$$g = P k_B T/2a \tag{4}$$

Forces on subunit i due to stretching and bending are obtained from the usual relation, $\mathbf{F}_i = -\nabla_i U$. Explicit expressions for the stretching and bending forces are given in the Appendix. Total direct forces are simply the sum of stretching and bending forces.

In order to simulate the Brownian diffusion of N identical spherical subunits, the method of Ermak and McCammon is used.[2] If the initial position of subunit i is $\mathbf{r}_i^0$, its position after a dynamics time step of duration Δt is given by

$$\mathbf{r}_i = \mathbf{r}_i^0 + \frac{\Delta t}{k_B T} \sum_{j=1}^{N} \mathbf{D}_{ij}^0 \cdot \mathbf{F}_j^0 + \mathbf{R}_i(\Delta t) \tag{5}$$

where $\mathbf{F}_j^0$ is the initial direct force acting on subunit j, $\mathbf{R}_i$ is a vector of Gaussian random numbers of zero mean and variance–covariance

$$\langle \mathbf{R}_i \mathbf{R}_j \rangle = 2\mathbf{D}_{ij}^0 \Delta t \tag{6}$$

and $\mathbf{D}_{ij}^0$ is the initial hydrodynamic interaction tensor between subunits i and j. In this work, the Rotne–Prager tensor[32] with stick boundary conditions is used to approximate $\mathbf{D}_{ij}^0$. The self terms are given by

$$\mathbf{D}_{ii} = (k_B T/6\pi\eta a)\mathbf{I} \tag{7}$$

where η is the solvent viscosity and $\mathbf{I}$ is the 3×3 identity tensor. Since different subunits may overlap, it is necessary to distinguish two special cases when $i \neq j$. For identical, but nonoverlapping, beads

$$\mathbf{D}_{ij} = \frac{k_B T}{8\pi\eta r_{ij}} \left[\left(\mathbf{I} + \frac{\mathbf{r}_{ij}\mathbf{r}_{ij}}{r_{ij}^2} \right) + \frac{2a^2}{r_{ij}^2} \left(\frac{1}{3}\mathbf{I} - \frac{\mathbf{r}_{ij}\mathbf{r}_{ij}}{r_{ij}^2} \right) \right] \tag{8}$$

where $\mathbf{r}_{ij} = \mathbf{r}_i - \mathbf{r}_j$ and $r_{ij} = |\mathbf{r}_{ij}|$. For identical, but overlapping, beads of radius a ($r_{ij} < 2a$)[32,33]

$$\mathbf{D}_{ij} = \frac{k_B T}{6\pi\eta a} \left[\left(1 - \frac{9}{32}\frac{r_{ij}}{a} \right)\mathbf{I} + \frac{3}{32}\frac{\mathbf{r}_{ij}\mathbf{r}_{ij}}{a r_{ij}} \right] \tag{9}$$

$\mathbf{R}_i(\Delta t)$ represents the stochastic displacement of subunit i due to collisions with solvent, and its construction is described elsewhere.[2,15] Each component of $\mathbf{R}_i$ consists of a linear combination of $3N$ normally distributed Gaussian random numbers ($\langle X_m \rangle = 0$, $\langle X_m X_n \rangle = 2\delta_{mn}\Delta t$). In many simulations $\mathbf{D}_{ij}^0$ was approximated by preaveraging.[29] In those cases, orientational preaveraging of a single chain configuration was achieved with

$$(\mathbf{D}_{ij})_{opa} = \mathbf{I}\ \mathrm{Tr}\ (\mathbf{D}_{ij})/3 \tag{10}$$

Since we are dealing with a flexible system, it is necessary to average eq 10 over all possible chain configurations. This was done by simply generating a large number of different chains (typically 500) and averaging eq 10. These averaged tensors were then used in eq 5 for subsequent dynamics.

In order to simulate a particular dynamics experiment, it is necessary to average an appropriate quantity for an ensemble of different structures as they evolve in time. The time evolution of a single chain, henceforth called a trajectory, is derived by successive application of eq 5. A dynamics time step, Δt, of 0.1 ns was used in most simulations since this is small enough to ensure essential constancy of direct forces for this model system. At regular time intervals during a trajectory, τ (τ is a variable integral multiple of Δt), quantities related to experimental observables are computed. For the particular example of fluorescences depolarization from a dye molecule rigidly bound to the chain, the relevant quantity is

$$F(j\tau, k\tau) = P_2(\mathbf{u}(j\tau)\cdot\mathbf{u}(k\tau)) \tag{11}$$

where P_2 is the second-order Legendre polynomial and $\mathbf{u}(j\tau)$ is a unit vector along the absorption/emission dipole

at time $j\tau$. Because the time average of F is a stationary quantity,[34] the following average is computed:

$$\langle F(j\tau)\rangle_t = \frac{1}{n-j+1}\sum_{k=0}^{n-j} F((k+j)\tau,k\tau) \qquad (12)$$

where the subscript t denotes a time average of a single trajectory and n denotes the final experimental time step of a trajectory. This procedure is repeated on an ensemble (typically 100–500) of different chains and the following average is computed:

$$F(j\tau) = \langle\langle F(j\tau)\rangle_t\rangle_e = (1/m)\sum_{j=1}^{m}\langle F(j\tau)\rangle_t \qquad (13)$$

where the subscript e denotes an ensemble average over m different trajectories. For the special case of fluorescence depolarization with collinear absorption and emission dipoles, F is related directly to the polarization anisotropy given by[35,36]

$$r(t) = 0.4\langle P_2(\mathbf{u}(t)\cdot\mathbf{u}(0))\rangle = 0.4F(t) \qquad (14)$$

The additional case of depolarized light scattering is treated in a subsequent section. It should be emphasized that several different "experiments" can be carried out in the same simulation.

In order to quantify the reproducibility of an experiment, each simulation is broken down into a number of equivalent but independent subsimulations (usually 4 or 5). Overall averages and standard deviations (σ_F) are then computed from the $F(t)$'s derived from the subsimulations. By the use of the central limit theorem,[37] the standard deviation in $F(t)$ for the entire simulation is taken to be equal to $\sigma_F/(n_s)^{1/2}$, where n_s is the number of subsimulations. The error bars in the figures on certain data points correspond to these standard deviations.

III. Results and Discussion

A. Stretching Forces. In previous work,[17] a model similar to the one employed here was used. The difference between them involves replacement of rigid-body constraints (fixed virtual bond lengths betwen adjacent subunits) with harmonic potentials. In general, the conformational statistics and dynamics of the rigid and flexible models are different even in the limit of an infinitely large force constant.[38-40] The conformational statistics and to a lesser extent the dynamics of the rigid model can be corrected to yield those of the corresponding flexible model by adding a compensating metric (Fixman) potential.[1,5,38,40] In recent studies of a butane-like model, Perchak et al. demonstrated that the dynamics of flexible and rigid models are indistinguishable in the high-friction limit.[40] Alternatively, the SHAKE algorithm[41] or extensions thereof[15,42] can be used in simulations on rigid models.[15,17,43] This algorithm not only enforces constraints but attempts to do so in a dynamically rigorous manner.

Stretching forces were used in this work to circumvent the necessity of using computationally expensive constraint algorithms[15,17] and also to account for the finite extensibility of real chain molecules. On the other hand, the use of stretching forces may necessitate taking short Δt's (especially for large h) in order to ensure essential constancy of those forces during a dynamics step. Indeed, rapid bond vibrations in molecular dynamics provided the initial motivation to develop substitute constraint methods.[41]

In order to estimate the range of allowed Δt's for our model on the basis of stretching forces alone, consider a bead of radius a = 15.9 Å in an aqueous media at 20 °C that is harmonically bound at the origin by a spring with force constant $h = \alpha k_B T/b^2$, where α is a dimensionless constant and $b = 2a$. The one-dimensional displacement of the bead in time Δt is approximately $\Delta x \simeq D\Delta t F^0/k_B T = -\alpha D\Delta t x^0/b^2$, where x^0 is the initial displacement. The mean square displacement of the bead is $\langle x^2\rangle = k_B T/h = b^2/\alpha$. For sake of illustration, assume α = 100, $x^0 = (2b^2/\alpha)^{1/2}$ = 4.51 Å, and Δt = 0.1 ns. This yields Δx = −0.60 Å. The magnitude of the force will change by 13% under these conditions. This can be reduced by reducing Δt or α.

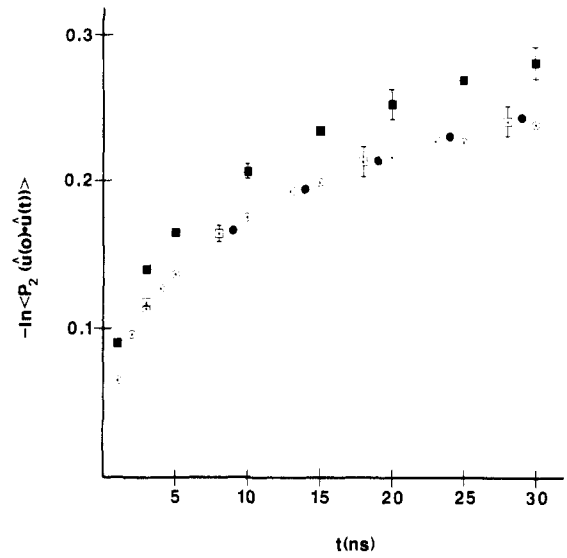

Figure 2. Effect of stretching force constant, h, on fluorescence depolarization. In all cases, P = 600 Å, Δt = 0.1 ns, and N = 10 beads. Reduced force constants are hb^2/k_BT = 100 (●), 10 (⊡), 4(■). Dotted circles are for rigid constraints using the SHAKE-HI algorithm (ref 17).

Figure 2 shows the effect of varying h on simulated fluorescence depolarization (fd) experiments. The wlc consists of 10 beads (a = 15.9 Å) with P = 600 Å. Each simulation represents the average of 100 trajectories, and Δt = 0.1 ns. The absorption and emission dipole was placed at the center of the chain collinear with the central virtual bond (unit vector $\mathbf{u}(t)$). Shown are the results using three different force constants as well as rigid-body constraints (0). Except for the weak force constant case with $h = 4k_BT/b^2$, they are in excellent agreement with each other. These results are consistent with those of other investigators.[40] In all subsequent work reported here, a value of $h = 100k_BT/b^2$ is used.

B. Preaveraged Hydrodynamic Interaction. With the 10-bead wlc model described in section IIIA, parallel simulations with and without peraveraging were carried out, and the results for fluorescence depolarization are shown in Figure 3. Within the uncertainty of the simulations, preaveraging has no noticeable effect. From a computational standpoint, it is highly advantageous to preaverage hydrodynamic interactions (HI).

Without preaverging, it is necessary to recompute the configuration-dependent $\mathbf{D}_{ij}$'s repetitively during the time course of a simulation. Furthermore, in order to calculate the stochastic displacements, $\mathbf{R}_i(\Delta t)$, which satisfy eq 6, one must calculate a $3N \times 3N$ matrix (N is the number of subunits) that is essentially the "square root" of the generalized $3N \times 3N$ diffusion matrix.[2,4,15] The number of calculations required to calculate the diffusion matrix and its "square root" varies as N^2 and N^3, respectively. (However, Fixman[4] has devised an algorithm in which computation of the $\mathbf{R}_i$'s varies as N^2.) Since computing these quantities is rate-limiting for dynamics, computation time increases approximately as $N^2 - N^3$, which limits one

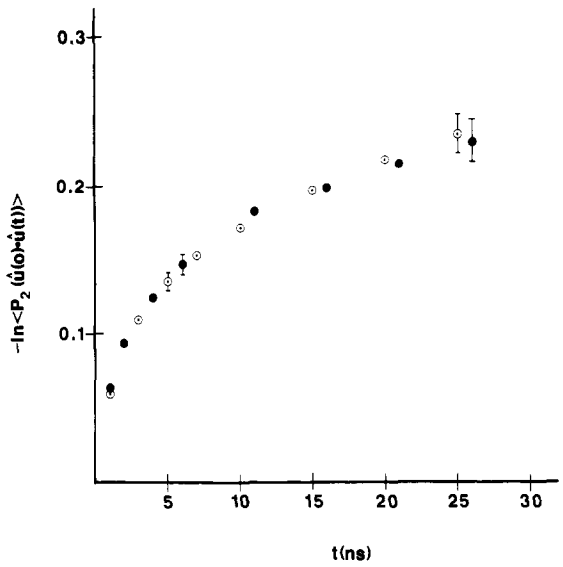

Figure 3. Effect of preaveraging hydrodynamic interaction on fluorescence depolarization of 10-subunit chains. Filled and dotted circles represent no preaveraging and preaveraging, respectively. In both cases, P = 600 Å, Δt = 0.1 ns, and hb^2/k_BT = 100.

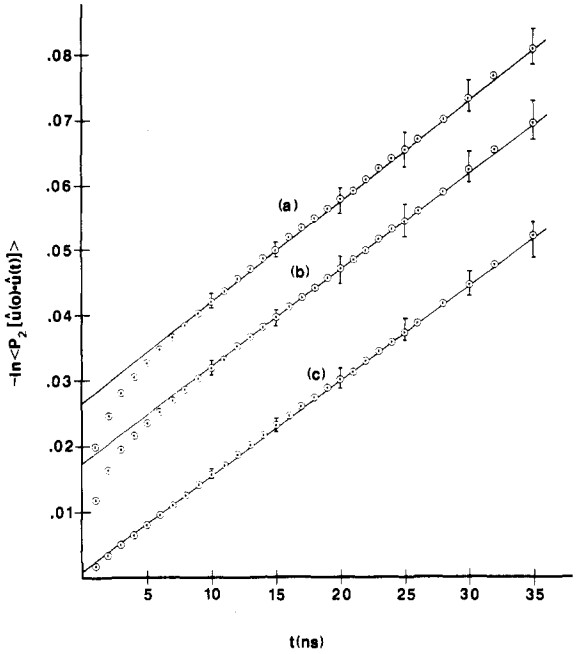

Figure 4. Rotational diffusion of a nearly rigid rod with preaveraging of hydrodynamic interaction. All three curves are from the same simulation with P = 5000 Å, Δt = 0.025 ns, hb^2/k_BT = 100, and N = 10 beads. In (a), (b), and (c) **u** is a unit vector between nearest-neighbor subunits in the center of the chain, next to nearest-neighbor subunits in the center of the chain, and the first and last subunits, respectively. Apparent rotational diffusion constants (slope = $6D_R$) of 2.58 × 10^5, 2.47 × 10^5, and 2.42 × 10^5 s^{-1} are obtained for slopes (a), (b), and (c), respectively.

to fairly short chains. In the case of preaveraged HI, on the other hand, it is necessary to compute the diffusion and "square root" matrices only once. For wormlike chains, computation time will vary as N, making simulations of much longer chains possible.

To illustrate that preaveraging in Brownian dynamics yields accurate *overall* rotational diffusion constants, simulations were carried out on nearly rigid rods, and the results are shown in Figure 4. From the slopes of these curves (=$6D_R$ where D_R is the rotational diffusion constant), D_R = 2.58 × 10^5; 2.47 × 10^5, and 2.42 × 10^5 s^{-1} for a, b, and c, respectively. Using other methods, Garcia de la Torre and co-workers[29] obtain 2.48 × 10^5 and 2.57 × 10^5 s^{-1} with and without preaveraging, respectively, for a rigid array of 10 beads (a = 15.9 Å, T = 293 K, η = 0.010 02 P). Because of the statistical uncertainty inherent in the simulation method, it would be difficult to distinguish the 3.4% discrepancy between the preaveraged and nonpreaveraged rotational diffusion constants of this structure. Incidentally, a relatively short time step was used in this particular simulation to ensure constancy of *bending* forces. According to eq 4, a persistence length of 5000 Å requires a large g.

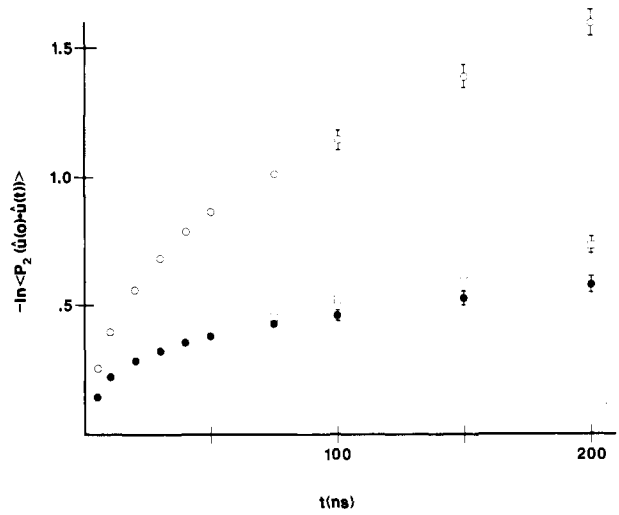

Figure 5. Fluorescence depolarization from chromophores bound to different sites on a 30-subunit chain. **u** is a unit vector between adjacent subunits. Filled circles correspond to **u** vectors at the center of the chain, unfilled squares to the third **u** vectors from the chain ends, and unfilled circles to the **u** vectors at the end of the chain. P = 400 Å, Δt = 0.1 ns, and hb^2/k_BT = 100.

C. Thirty-Subunit Wormlike Chains. Preaveraging HI and using stretching forces instead of rigid-body constraints have made it possible to carry out simulations on much longer chains. Figure 5 represents fluorescence depolarization from a 30-subunit chain (L = 922 Å) with P = 600 Å. As before, the emission dipole is taken to be collinear with a virtual bond vector. There is considerably more motion at the very end of the chain (○) than at the center (●). However, these end effects fall off rapidly as one moves into the chain. The squares (□) correspond to a dipole located approximately 60 Å from the chain end, and for times less than about 80 ns, the results are indistinguishable from those of a dipole located at the chain center. At longer times, however, end effects become noticeable, which may be an important factor in experiments like triplet anisotropy decay,[44,45] where excited-state lifetimes are long. If the wlc's were behaving as truly rigid bodies, considerably less depolarization would occur. From the work of Hagerman and Zimm,[30] one can determine $\langle D_R \rangle$ = 2.48 × 10^4 s^{-1} for an ensemble of "frozen" 30-subunit wlc's with this persistence length. For rigid wlc's with this assumed dipole geometry[35,36]

$$-\ln \langle P_2 \mathbf{u}(0)\cdot\mathbf{u}(t)\rangle = 6\langle D_R\rangle t \qquad (15)$$

At 200 ns, $6\langle D_R\rangle t$ = 0.030, which is substantially lower than the value observed for flexible chains.

The effect of P on fd is shown in Figure 6. Except for differences in P, the model parameters are identical with those of the previous figure. Evidently, fd is very sensitive to chain stiffness, particularly when P is less than about 500 Å.

The simulated results shall now be compared with the Barkley–Zimm theory of bending.[25] In this model, the wlc is represented as a very long elastic cylinder with a

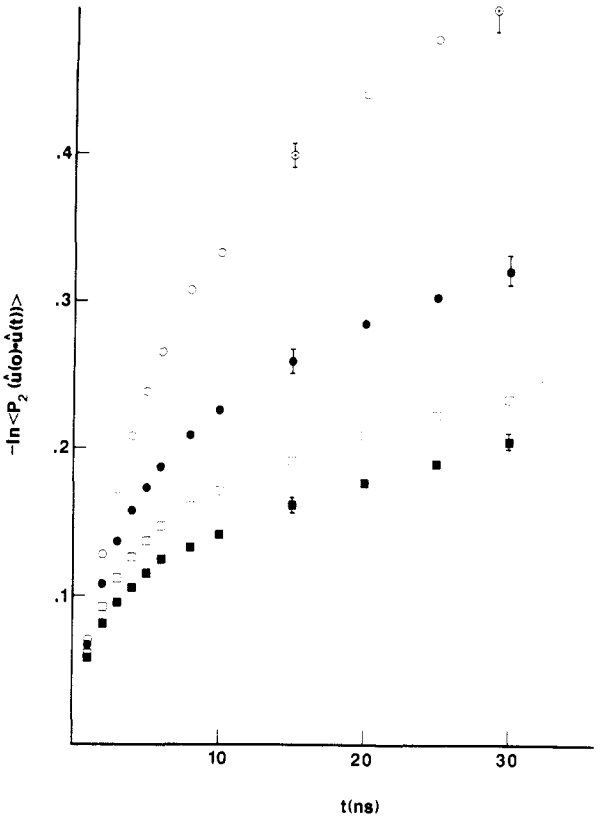

Figure 6. Effect of P on fluorescence depolarization from 30-subunit wormlike chains. **u** is a unit vector located at the chain center. P (Å) = 200 (○); 400 (●); 600 (□); 800 (■). Other parameters are the same as in Figure 5.

fluorescent probe attached at its center. A cylinder radius of 13 Å and P = 400 Å were used in the Barkley–Zimm theory for comparison. To suppress the contribution of overall rotation, $6\langle D_R\rangle t$ is subtracted from the data of Figure 5 (filled circles). As shown in Figure 7, the results are in excellent agreement with each other despite differences in the two models. As pointed out by Schurr,[35] however, the anisotropy expression of Barkley and Zimm is incorrect (eq IV.11 of ref 25). For the special geometry used in this work, the correct anisotropy expression is

$$r(t) = 0.4\langle P_2\mathbf{u}(0)\cdot\mathbf{u}(t)\rangle = 0.4\exp(-3\Delta(t)/2) \quad (16)$$

where $\Delta(t)$ is the bending function of Barkley and Zimm. Equation 16 along with eq IV.16a of ref 25 was used to obtain the X's in Figure 7. The contribution of overall rotation was subtracted from the simulated results since eq IV.16a of ref 25 represents the contribution of internal bending (see eq III.21[25]). According to a reviewer, however, eq IV.16a leads to an overestimate in $\Delta(t)$ by about $2\langle D_R\rangle t$ and this occurs as a result of replacing a sum by an integral in the derivation of eq IV.16a. The leading correction term in the Euler–McLaurin summation formula for $\Delta(t)$ is approximately $-2\langle D_R\rangle t$. Substracting $2\langle D_R\rangle t$ from the crosses in Figure 7 lowers them by 2.48×10^{-3}, 4.96×10^{-3}, and 9.92×10^{-3} at t = 50, 100, and 200 ns, respectively. In any case, this correction is a minor one.

A similar comparison was made previously between the Barkley–Zimm theory and simulations on a 10-subunit wlc but with P = 600 Å.[17] Although the agreement between them was quite good, the simulated fd results were lower than predicted by the Barkley–Zimm Theory. This discrepancy was attributed to long-range relaxations present in long chains but absent in short ones. The present results also appear to rule out the possibility that tensile forces acting along the chain reduce the amplitude of bending

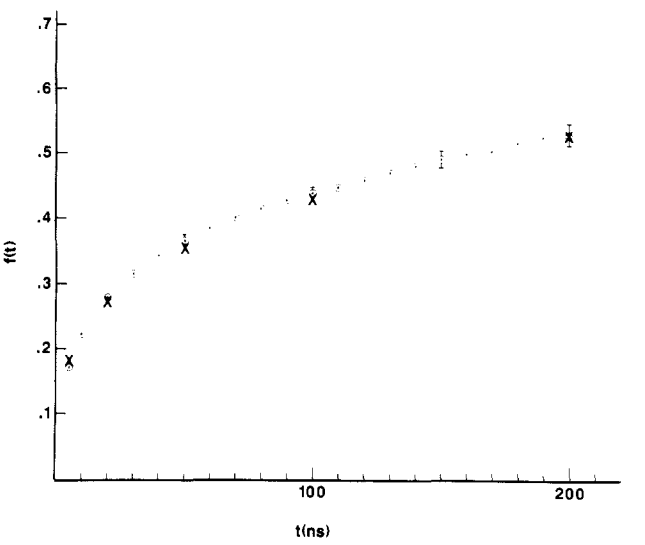

Figure 7. Comparison with the Barkley–Zimm Theory. Data points from the simulation (○) are those of Figure 5 with the contribution of overall bending subtracted out. Crosses (X) denote the Barkley–Zimm Theory. $f(t) = -\ln\langle P_2(\mathbf{u}(0)\cdot\mathbf{u}(t))\rangle - 6\langle D_R\rangle_{frozen}t$.

in long chains. On the basis of these results, it is concluded that the bending theory of Barkley and Zimm[25] is accurate at short times, provided the dynamics of the chain interior is of interest. It was assumed that the emission dipole of the fluorescent chromophore is collinear with the chain backbone to eliminate contributions due to torsional motions that are adequately described by analytic theories.[25,26,43] From experimental fd studies of ethidium bromide bound to DNA, it is possible to deduce a torsional rigidity of about $C = 1.3\times10^{-19}$ erg cm.[22-24,46] This is significantly lower than the values of 2.4×10^{-19} and 2.9×10^{-19} erg cm obtained from rates of ring-closure[47] and DNA supercoiling[48] studies, respectively. In the fd studies, however, the contribution of internal bending has been ignored in the past. Including it would increase C and reconcile, to a large extent, the differences between fd and other methods (Schurr, J. M., private communication).

With regards to low-angle depolarized light scattering (dls), the chain is modeled as $N-1$ anisotropic scattering elements each with two distinct polarizability components parallel and perpendicular to the corresponding virtual bond vector. The relevant average in this case is a reduced dynamic structure factor defined by[49]

$$G(t) = \frac{1}{(N-1)^2}\sum_{i=1}^{N-1}\sum_{j=1}^{N-1}\langle P_2(\mathbf{u}_i(0)\cdot\mathbf{u}_j(t))\rangle \quad (17)$$

where $\mathbf{u}_j(t)$ is a unit vector along with jth virtual bond at time t. Unlike fd (eq 14), correlations between different scattering elements contribute to dls. In the special case of rigid structures, the dynamical behavior of $r(t)$ and $G(t)$ is identical (i.e., $r(t)/r(0) = G(t)/G(0) = \exp(-6\langle D_R\rangle t)$). This, however, is not the case for flexible structures. Simulated dls results for a 30-subunit wlc with P = 400 Å are shown in Figure 8. Both fd (Figure 5) and the dls (Figure 8) experiments were carried out in the same simulation. However, the fd experiment is far more sensitive to rapid internal motion than dls. Evidently, only the slower collective and overall motions are correlated between two scattering elements that are relatively far apart from each other. Since these terms dominate dls from long chains, this experiment is not as sensitive to local motions as fd. However, dls is not entirely insensitive to local motions. From the long-time slope of Figure 8, equating it to $6\langle D_R\rangle$, we obtain $\langle D_R\rangle = 8.3\times10^4$ s^{-1}, which is

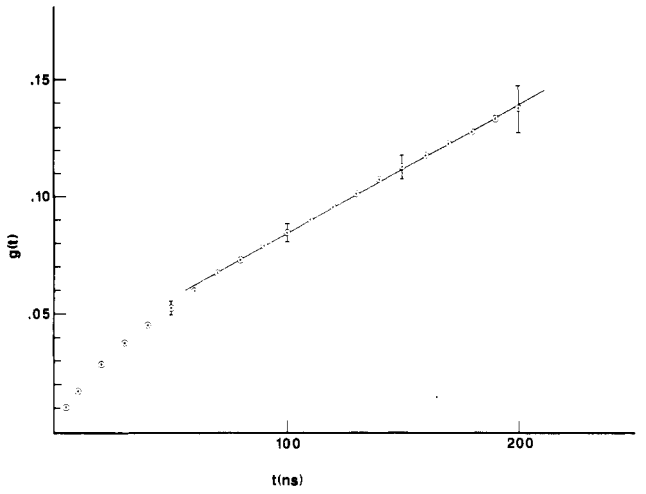

Figure 8. Depolarized light scattering from 30-subunit chains. Parameters are the same as in Figure 5. $g(t) = -\ln [G(t)/G(0)]$.

substantially higher than the "frozen" value of 2.48×10^4 s^{-1}.[30] There is apparently still internal motion in dls at times of 100–200 ns.

IV. Summary

Simulations have been carried out of fluorescence depolarization and depolarized light scattering with a discrete wormlike chain model of up to 30 subunits. It was found that replacing rigid-body constraints with harmonic constraints does not affect the results of the two experiments unless the stretching force constant is set very low. Preaveraging hydrodynamic interaction was found to have a negligible effect on fluorescence depolarization from 10-subunit wormlike chains. Preaveraging HI made it feasible to carry out the simulations on 30-subunit chains.

The fd simulations indicate a considerable amount of internal motion as well as a high degree of sensitivity to the flexibility of the wormlike chain. The simulation results are found to be in excellent agreement with the bending theory of Barkley and Zimm[25] when the chromophore is placed near the center of the chain. Depolarized light scattering was found to be less sensitive to internal motion. Nonetheless, internal motion is still present at the short times explored in this work.

The number of trajectories carried out in a simulation ranged from 100 to 500. The number of trajectories required to obtain high accuracy depends to some extent on the "experiment". For example, to achieve comparable statistics in depolarized light scattering and fluorescence depolarization, about 4 times the number of trajectories have to be carried out in the former experiment.

Acknowledgment. The author thanks Professors J. M. Schurr and J. A. McCammon for helpful discussions. S.A.A. is the recipient of a Presidential Young Investigator Award, a Camille and Henry Dryfus Grant for Newly Appointed Faculty in Chemistry, a grant from Research Corp., and a PRF Type G Starter Grant from the American Chemical Society.

Appendix

Let $\mathbf{u}_j = \mathbf{b}_j/b_j$ denote the unit vector between subunits j and $j+1$. Stretching forces are given by

$$\mathbf{F}_1^{s} = h(b_1 - 2a)\mathbf{u}_1$$

$$\mathbf{F}_j^{s} = -h(b_{j-1} - 2a)\mathbf{u}_{j-1} + h(b_j - 2a)\mathbf{u}_j \qquad 2 \le j \le N-1$$

$$\mathbf{F}_N^{s} = -h(b_{N-1} - 2a)\mathbf{u}_{N-1} \qquad \text{(A-1)}$$

The bending forces turn out to be

$$\mathbf{F}_1^{b} = -g(\mathbf{u}_2 - \mathbf{u}_1)/b_1$$

$$\mathbf{F}_2^{b} = g(\mathbf{u}_2 - \mathbf{u}_1)(1/b_1 + 1/b_2) - g(\mathbf{u}_3 - \mathbf{u}_2)/b_2$$

$$\mathbf{F}_j^{b} = -g(\mathbf{u}_{j-1} - \mathbf{u}_{j-2})/b_{j-1} + g(\mathbf{u}_j - \mathbf{u}_{j-1}) \times (1/b_{j-1} + 1/b_j) - g(\mathbf{u}_{j+1} - \mathbf{u}_j)/b_j \qquad 3 \le j \le N-2$$

$$\mathbf{F}_{N-1}^{b} = -g(\mathbf{u}_{N-2} - \mathbf{u}_{N-3})/b_{N-2} + g(\mathbf{u}_{N-1} - \mathbf{u}_{N-2})(1/b_{N-2} + 1/b_{N-1})$$

$$\mathbf{F}_N^{b} = -g(\mathbf{u}_{N-1} - \mathbf{u}_{N-2})/b_{N-1} \qquad \text{(A-2)}$$

In order to derive these bending forces, it is necessary to assume that the angle between adjacent virtual bond vectors is small, or in other words, $\mathbf{u}_j \cdot \mathbf{u}_{j+1} \simeq 1$. In the special case of constant bond length, these forces simplify to yield the Harris–Hearst bending forces.[50]

References and Notes

(1) Fixman, M.; Kovac, J. *J. Chem. Phys.* **1974**, *61*, 4939, 4950.
(2) Ermak, D.; McCammon, J. A. *J. Chem. Phys.* **1978**, *69*, 1352.
(3) Fixman, M. *J. Chem. Phys.* **1978**, *69*, 1527, 1538.
(4) Fixman, F. *Macromolecules* **1981**, *14*, 1710.
(5) Pear, M.; Weiner, J. H. *J. Chem. Phys.* **1979**, *71*, 212.
(6) Helfand, E.; Wasserman, Z. R.; Weber, T. A. *Macromolecules* **1980**, *13*, 526.
(7) Helfand, E.; Wasserman, Z. R.; Weber, T. A., Skolnick, J.; Runnels, J. H. *J. Chem. Phys.* **1981**, *75*, 4441.
(8) Perchak, D.; Weiner, J. H. *Macromolecules* **1981**, *14*, 785.
(9) Pear, M.; McCammon, J. A. *J. Chem. Phys.* **1981**, *74*, 6922.
(10) McCammon, J. A.; Gelin, B. R.; Karplus, M.; Wolynes, P. G., *Nature (London)* **1976**, *262*, 325.
(11) McCammon, J. A.; Northrup, S. H.; Karplus, M.; Levy, R. M. *Biopolymers* **1980**, *19*, 2033.
(12) James, C.; Evans, G. T. *J. Chem. Phys.* **1982**, *76*, 2680.
(13) Northrup, S. H.; Allison, S. A.; McCammon, J. A. *J. Chem. Phys.* **1984**, *80*, 1517.
(14) Allison, S. A.; Srinivasan, N.; McCammon, J. A.; Northrup, S. H. *J. Phys. Chem.* **1984**, *88*, 6152.
(15) Allison, S. A.; McCammon, J. A. *Biopolymers* **1984**, *23*, 167.
(16) Harvey, S. C.; Cheung, H. C. *Biopolymers* **1980**, *19*, 913.
(17) Allison, S. A.; McCammon, J. A. *Biopolymers* **1984**, *23*, 363.
(18) McCammon, J. A. *Rep. Prog. Phys.* **1984**, *47*, 1.
(19) Kirkwood, J. G. "Macromolecules"; Auer, P. L., Ed.; Gordon and Breach: New York, 1967.
(20) Zimm, B. H. *J. Chem. Phys.* **1956**, *24*, 269.
(21) Wahl, Ph.; Paoletti, J.; Le Pecq, J. B. *Proc. Natl. Acad. Sci. U.S.A.* **1970**, *65*, 417.
(22) Thomas, J. C.; Allison, S. A.; Appellof, C. J.; Schurr, J. M. *Biophys. Chem.* **1980**, *12*, 177.
(23) Millar, D. P.; Robbins, R. J.; Zewail, A. *Proc. Natl. Acad. Sci. U.S.A.* **1980**, *77*, 5593.
(24) Hurley, I.; Osei-Gymiah, P.; Archer, S.; Scholes, C. P.; Lerman, L. S. *Biochemistry* **1982**, *21*, 4999.
(25) Barkley, M. D.; Zimm, B. H. *J. Chem. Phys.* **1979**, *70*, 2991.
(26) Allison, S. A.; Schurr, J. M. *Chem. Phys.* **1979**, *41*, 35.
(27) Yamakawa, H.; Yoshizaki, T. *J. Chem. Phys.* **1983**, *78*, 572.
(28) Yoshizaki, T.; Fujii, M.; Yamakawa, H. *J. Chem. Phys.* **1985**, *82*, 1003.
(29) Garcia de la Torre, J.; Lopez, M. C.; Tirado, M. M.; Friere, J. J. *Macromolecules* **1983**, *16*, 1121.
(30) Hagerman, P. J.; Zimm, B. H. *Biopolymers* **1981**, *20*, 1481.
(31) Schellman, J. *Biopolymers* **1974**, *13*, 217.
(32) Rotne, J.; Prager, S. *J. Chem. Phys.* **1969**, *50*, 4831.
(33) Garcia de la Torre, J.; Bloomfield, V. A. *Q. Rev. Biophys.* **1981**, *14*, 81.
(34) McQuarrie, D. A. "Statistical Mechanics"; Harper and Row: New York, 1976.
(35) Schurr, J. M. *Chem. Phys.* **1984**, *84*, 71.
(36) Szabo, A. *J. Chem. Phys.* **1984**, *81*, 150.
(37) Hogg, R. V.; Tanis, E. A. "Probability and Statistical Inference"; Macmillan: New York, 1977.
(38) Fixman, M. *Proc. Natl. Acad. Sci. U.S.A.* **1974**, *71*, 3050.
(39) Helfand, E. *J. Chem. Phys.* **1979**, *71*, 5000.
(40) Perchak, D.; Skolnick, J.; Yaris, R. *Macromolecules* **1985**, *18*, 519.

(41) Ryckaert, J. P.; Ciccotti, G.; Berendsen, H. J.; J. Comput. Phys. 1977, 23, 327.
(42) Ciccotti, G.; Ferrario, M.; Ryckaert, J. P. Mol. Phys. 1982, 47, 1253.
(43) van Gunsteren, W. F.; Karplus, M. Macromolecules 1982, 15, 1528.
(44) Hogan, M.; Wang, J.; Austin, R. H.; Monitto, C. L.; Hershkowitz, S. Proc. Natl. Acad. Sci. U.S.A. 1982, 79, 3518.
(45) Hogan, M.; Le Grange, J.; Austin, R. H. Nature (London) 1983, 304, 752.
(46) Thomas, J. C.; Schurr, J. M. Biochemistry 1983, 22, 6194.
(47) Shore, D.; Baldwin, R. L. J. Mol. Biol. 1983, 170, 957, 983.
(48) Horowitz, D. S.; Wang, J. C. J. Mol. Biol. 1984, 173, 75.
(49) Carpenter, D. K.; Skolnick, J. Macromolecules 1981, 14, 1284.
(50) Harris, R. A.; Hearst, J. E. J. Chem. Phys. 1966, 44, 2595.

Static and Dynamic Properties of Polystyrene in Good Solvents: Ethylbenzene and Tetrahydrofuran

K. Venkataswamy and A. M. Jamieson*

Department of Macromolecular Science, Case Western Reserve University, Cleveland, Ohio 44106

R. G. Petschek

Department of Physics, Case Western Reserve University, Cleveland, Ohio 44106.
Received January 25, 1985

ABSTRACT: We report static and dynamic light scattering studies of polystyrenes of narrow molecular weight distribution in ethylbenzene (EtPh) and tetrahydrofuran (THF) as solvents. These experiments generate values for z-average radius of gyration, $\langle R_g \rangle_z$, weight-average second osmotic virial coefficient, A_2, z-average translational diffusion coefficients, $\langle D_t \rangle_z$, and hence the diffusion virial coefficients, k_D, and the z-average of the inverse frictional radius, $\langle R_f^{-1} \rangle_z$. The results show that while for a specific molecular weight the $\langle R_g \rangle_z$ values in THF are similar to our experimental values in ethylbenzene and to literature values in benzene or toluene, the A_2 values, as well as hydrodynamic radii, are substantially larger for THF. We find that values of "universal ratios" of static and dynamic quantities in ethylbenzene are in good agreement with predictions of renormalization group theory appropriate to the nondraining good-solvent limit, while those for THF are *not*. We present a more stringent test of universality by plotting the static light scattering data directly in a "scaling" form. Identical polystyrene samples in THF and ethylbenzene are clearly different when analyzed in this way, although they do conform to an empirical universal description for solvents of arbitrary quality. These analyses suggest that in THF polystyrene exists in a more flexible conformation and is closer to the nondraining, good-solvent limit.

Background

Interest in measurements of the transport properties of polymer chains in good solvents has revived recently because of new theoretical developments that have established procedures by which realistic predictions of experimental parameters can be made for such systems. On the one hand, numerical simulations of chain dynamics, usually using Monte Carlo methods previously confined to Gaussian chains,[1,2] can now be extended to self-avoiding walks,[3-5] thus enabling one to incorporate the excluded-volume effect. On the other hand, successful application of renormalization group (RG) techniques[6] to describe features of polymer chain statistics with excluded volume[7,8] have led recently to RG calculations of polymer hydrodynamic parameters.[9-12]

Theory predicts[7,9] and experiment appears to confirm[13,14] that structural radii, R, exhibit power scaling laws against molecular weight, M, of the form

$$R \sim M^{\nu} \tag{1}$$

where ν is a characteristic exponent. For Gaussian coils, $\nu = 0.5$ and, as solvent quality increases, ν rises smoothly to the asymptotic value $\nu = 0.588$. Experiment indicates[13,14] that the crossover occurs more sharply for the static radius $\langle R_g \rangle_z$ than for the hydrodynamic radii. Recent RG calculations further predict specific values for certain universal ratios of static and hydrodynamic parameters.[9] These are

$$\psi = \frac{A_2 M^2}{4\pi^{3/2} N_A \langle R_g^2 \rangle^{3/2}} \tag{2}$$

$$U_{A\eta} = \frac{A_2 M}{[\eta]} \tag{3}$$

$$U_{fs} = \frac{f}{\langle R_g^2 \rangle^{1/2} \eta_s} \tag{4}$$

$$U_{\eta s} = \frac{M[\eta]}{N_A \langle R_g^2 \rangle^{3/2}} \tag{5}$$

and

$$U_{\eta f} = \left(\frac{M[\eta]}{N_A} \right)^{1/3} \frac{\eta_s}{f} \tag{6}$$

where the frictional coefficient $f = 6\pi\eta_s R_f = kT/6\pi\eta_s D^0_t$ and D^0_t is the limiting translational diffusion coefficient. In eq 2-6, $[\eta]$ is the intrinsic viscosity, η_s is the solvent viscosity, N_A is Avogadro's number, k is the Boltzmann constant, and T is absolute temperature. These quantities have been calculated recently[9] for both the Θ and asymptotic good-solvent limit, the hydrodynamics being formulated within the Kirkwood-Riseman model with a full Oseen tensor description.

Polystyrene is one of the most widely studied polymers because of the availability of polymer samples of narrow

0024-9297/86/2219-0124$01.50/0